ISSN: 2688-8645

3D Finite Element Analysis of Knee Joint Stress Distribution Under Muscle Action with Partial ACL Rupture

Shize Pei

School of Mechanical Engineering, Shandong Key Laboratory of CNC Machine Tool Functional Components, Qilu University of Technology (Shandong Academy of Sciences), Jinan Shandong, 250353, China

838798394@qq.com

Abstract

This study aimed to investigate the impact of partial rupture of the anterior cruciate ligament (ACL) on the stress distribution within the meniscus and cartilage of the knee joint using finite element analysis. The findings provide a theoretical foundation for the clinical prevention and treatment of ACL injuries. The anteromedial bundle of the ACL is crucial for maintaining valgus stability in the knee during standing with the knee in extension. A reduction in valgus or rotational stability leads to a redistribution of stress within the joint, making the meniscus, as a cushioning structure, more susceptible to injury. Consequently, in sports requiring high knee rotational stability, clinicians should be vigilant for potential secondary meniscal injuries, particularly involving the anteromedial bundle, and consider early clinical intervention to mitigate further damage.

Keywords

Anterior Cruciate Ligament; Knee Joint; Finite Element Analysis; Meniscus; Articular Cartilage.

1. Introduction

The anterior cruciate ligament (ACL) is one of the primary ligamentous structures connecting the tibiofemoral joint, the main weight-bearing joint in the human body. The ACL plays a critical role in maintaining the anterior-posterior and rotational stability of the tibiofemoral joint, particularly during complex and high-speed movements such as knee flexion, semi-squatting, rapid acceleration, and sudden stops or turns. Additionally, due to its lower tensile strength compared to the posterior cruciate ligament, the ACL is more susceptible to injury, with a damage rate exceeding 50% in various knee injuries. ACL rupture is a common sports-related injury, with a high incidence in athletic competitions [1]. Notably, the annual incidence of ACL tears among athletes participating in sports programs is as high as 68.6 per 100,000 individuals [2]. ACL injuries compromise knee stability, alter knee movement patterns, and increase tension in the hip flexors [3]. Clinically, acute ACL injuries are frequently complicated by concomitant injuries to the medial meniscus and/or medial collateral ligament, while medial meniscus lesions often develop secondary to chronic ACL injuries [4]. In patients with ACL injuries, internal rotation of the tibia accompanied by posterior medial bone edema of the tibial plateau has been associated with unstable meniscal slope lesions [5]. Furthermore, the risk of failure in medial meniscus repair surgery is relatively higher compared to lateral meniscus repair [6]. A comprehensive understanding of the characteristics and influencing factors of ACL rupture and meniscal injuries can facilitate the development of effective preventive measures to reduce the risk of meniscal injuries and osteoarthritis.

ISSN: 2688-8645

In recent years, various computational models of the normal knee have been developed to predict the biomechanical behavior of the joint [5], [6], [7], [8], [9]. These studies have primarily focused on the effects of complete ACL rupture on various components of the knee joint. However, partial ACL rupture is frequently observed in clinical practice. PARK et al. [10] reported that arthroscopic examination of 76 patients with ACL injuries revealed selective bundle rupture in approximately one-third of the cases, with three-quarters of these patients exhibiting rupture of the anteromedial bundle and one-quarter exhibiting rupture of the posterolateral bundle. This knowledge gap raises concerns about potential overtreatment in current surgical paradigms [11], particularly given the controversy surrounding reconstruction indications for partial tears. While ACL reconstruction effectively prevents secondary injuries in complete ruptures [12], the biomechanical consequences of partial ACL deficiency on meniscocartilaginous load distribution remain poorly characterized.

The aim of this paper is to address this critical knowledge gap through development of a muscle action finite element model of the knee joint. We hypothesize that partial ACL rupture induces distinct stress redistribution patterns in the menisci and articular cartilage, creating biomechanical environments conducive to progressive tissue degeneration and secondary injury development. By quantifying load transfer alterations across different ACL injury subtypes, our findings will provide mechanistic insights to optimize treatment strategies for partial ACL injuries.

2. Methods

2.1. Materials

Computed tomography (CT) imaging data of the right knee joint from a 30-year-old healthy adult male (with no history of knee-related diseases) were obtained from the Department of Joint Surgery at the Second Hospital of Shandong University in March 2024. The scanning area encompassed 10 cm above and below the knee joint, resulting in 350-layer CT images with a slice thickness of 0.625 mm. The imaging data were acquired in DICOM format.

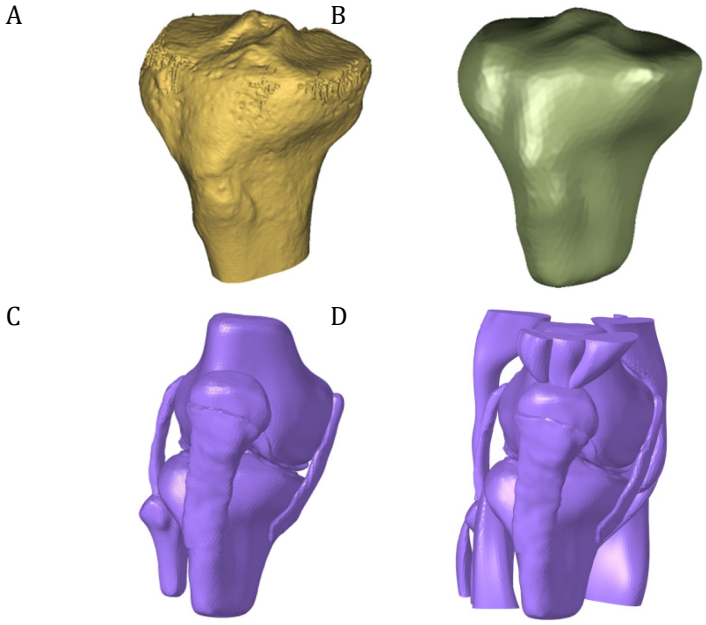

Fig 1. The process of 3D modeling of the knee joint. (A) Diagram after bone trimming, (B) Diagram after bone smoothing, (C) Model of knee joint, (D) Model of knee muscles

ISSN: 2688-8645

2.2. Finite Element Modeling

2.2.1. Construct the Three-dimensional Model of the Knee Joint

The two-dimensional (2D) CT image data in DICOM format were imported into Mimics 21.0 software (Materialise, Belgium). An appropriate threshold range was selected to identify bony structures based on the grayscale values of the image data. A region-growing algorithm was employed to generate a 2D digital model of each tissue structure, followed by 3D reconstruction to construct the 3D model. The 3D model of the knee joint skeleton was successfully generated from the CT image data. The surface of the initial 3D model was relatively rough and was refined using the Magics function within Mimics 21.0 software. The results of the refinement are illustrated in Fig. 1A.

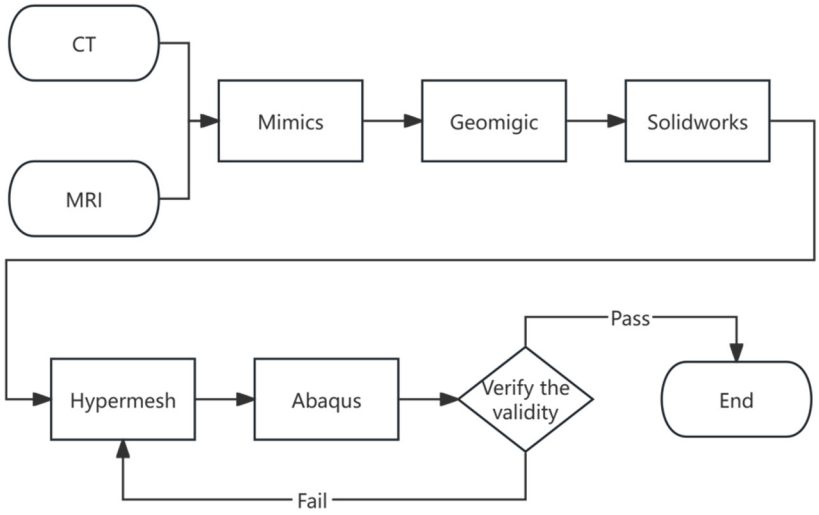

Fig 2. low of 3D modeling of knee joint

2.2.2. Smooth Processing of 3D Models of Knee Joints

The 3D model generated in Mimics 21.0 was characterized by a lamellar structure. To further optimize the model, STL format files of each tissue structure of the knee joint were imported into the reverse engineering software Geomagic Wrap 2021 (3D Systems, Inc., USA). The repair tool within the software was utilized to eliminate defects in the model and optimize its geometry. The smoothness and physical plausibility of the final model were ensured by applying the surface fitting command. After optimization optimization, the 3D models of bones and muscles were saved in STP format for subsequent finite element analysis. The results are shown in Fig. 1B.

2.2.3. Construction of Meniscus, Cartilage, Ligaments and Muscles

The generated STP format files were imported into SolidWorks software (Dassault Systèmes, Inc., USA) for further processing. Due to significant distortion in the meniscus extracted from the imaging data, a complete model of the medial and lateral meniscus of the knee was reconstructed based on the extracted meniscus contour and its morphological features. Additionally, a 3D model of the muscles surrounding the knee was created. In Mimics software, the "threshold" setting was optimized by adjusting the range of grayscale values to achieve effective separation of the bone and its surrounding tissues. The contour lines of cartilage and ligament tissues within the selected grayscale range were automatically marked, and the knee joint structures were manually delineated according to different sequences of image data, in conjunction with the physical morphology of human specimens, to ensure the authenticity and accuracy of the model. Two-dimensional images of the femoral cartilage, tibial cartilage, fibular cartilage, patellar ligament (PL), anterior cruciate ligament, posterior cruciate ligament (PCL), medial collateral ligament (MCL), and lateral collateral ligament (LCL) were constructed

ISSN: 2688-8645

separately. Different regions were segmented using a region-growing algorithm, and edge detection, selective editing, and hole filling were performed on each layer of the image to remove redundant data. Based on this, the 3D geometric model of the human knee joint was constructed using 3D computing technology. The detailed process of model construction is illustrated in Fig. 2.

2.2.4. 3D Model Meshing

Each tissue structure of the knee joint was exported as an STP file from Geomagic Wrap 2021 software and imported into Hypermesh 2020 software (Altair, USA) for geometry cleanup. In Hypermesh software, the soft tissues, muscles, bones, and ligaments of the knee joint were meshed, with mesh types selected and mesh quality verified. Bones and ligaments were meshed using tetrahedral elements of type C3D10M, with mesh sizes of 5 mm for the femur, tibia, and fibula, 3 mm for the patella, and 1 mm for the ligaments. Soft tissues and muscles were meshed using tetrahedral elements of type C3D4, with a mesh size of 6 mm.

Based on the above methodology, a model of the knee joint in extension (Fig. 1C) as well as a model of the knee muscles (Fig. 1D) were constructed. Each knee model represented four different anterior cruciate ligament states (Fig. 3), specifically: intact ACL, ruptured posterior lateral bundle of the ACL, ruptured anterior medial bundle of the ACL, and complete absence of the ACL.

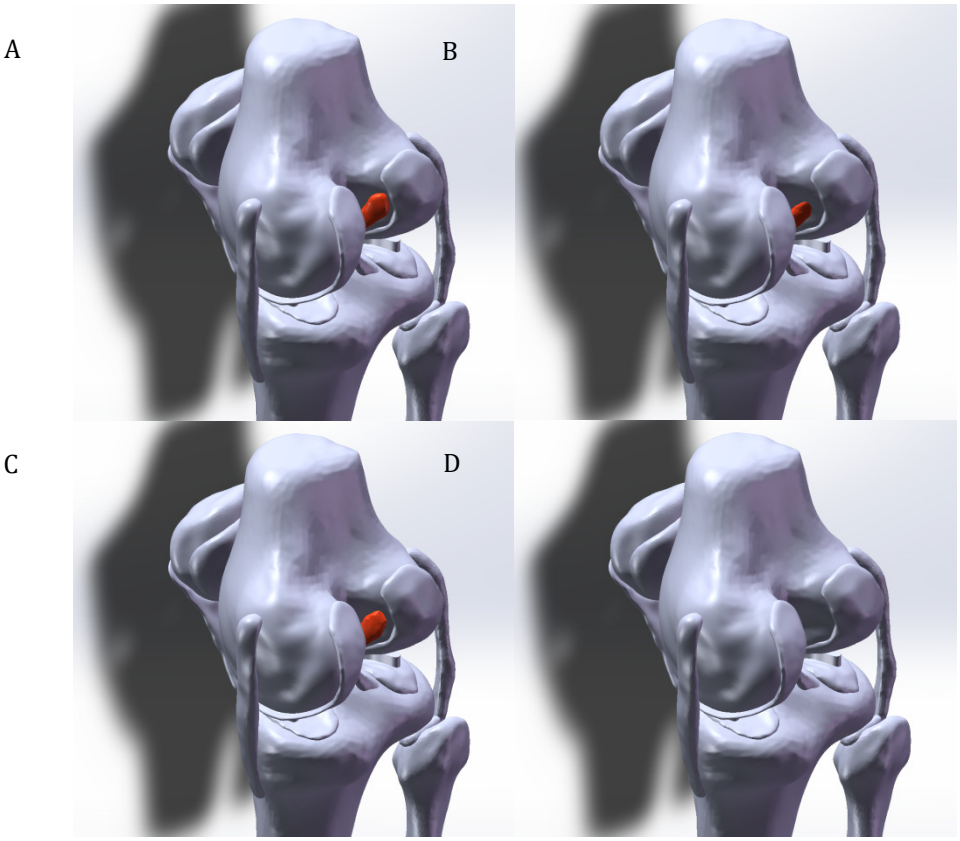

Fig 3. Knee models with intact ACL and varying degrees of damage to the knee joint. (A) Intact anterior cruciate ligament, (B) Rupture of the posterior lateral bundle of the anterior cruciate ligament, (C) Rupture of the anterior medial bundle of anterior cruciate ligament, (D) Missing anterior cruciate ligamen

2.2.5. Defining Structural Properties

The material properties of each knee joint structure significantly influence the outcomes of finite element analysiswhen studying the biomechanical properties of knee ligaments. To ensure the validity of the results, the mechanical material properties of each knee joint structure were derived from prior literature [13]. Bone material was modeled as rigid, as bone

ISSN: 2688-8645

tissue deformation is negligible in practice. The elastic modulus was set to 17,000 MPa, Poisson's ratio to 0.3, and density to 1,900 kg/m^3. Muscle tissue itself has a strong tensile ability, the ability to carry compressive loads is very limited, so muscle tissue according to their own muscle fiber direction is more orthogonal anisotropy [15], that is, along the direction of the muscle fibers more muscle stretching ability, perpendicular to the direction of the muscle fibers more muscle compression ability, muscle is defined as Holzapfel superelastic material,C10=0.6 kPa,k1=0.4 MPa,k2=35,κ=0.28,and density to 1,600 kg/m^3. Joint soft tissues and ligaments were defined as superelastic materials [15], with the Neo-Hookean model selected. The Neo-Hookean function is as follows [13]:

$$\psi = \frac{1}{2D} ln(\int)^2 + C_1(\bar{I}_1 - 3) + F_2(\lambda) \quad (1)$$

where C_1 is Neo-Hooke's constant and $\frac{1}{D}$ is the Bulk Modulus.

Table 1. Soft tissue and ligament material properties of the knee joint

Tissue structure	C_1	D	Density(kg/m^3)
Soft tissue	0.00347	12.4	1100
ACL	1.95	0.00683	1000
PCL	3.25	0.0041	1000
LCL	1.44	0.00126	1000
MCL	1.44	0.00126	1000

2.2.6. Boundary Conditions, Loads and Validation

In this knee model, the meniscus, articular cartilage, and surrounding muscle tissue were integrated into homogenized soft tissue, while preserving the bone and ligament structures. The femur remained unconstrained, while motion control of the tibia was achieved by constraining its three translational degrees of freedom and flexion degrees of freedom [16].The anterior and posterior corners of the meniscus were connected to the tibial plateau, and the ends of each ligament were attached to the femur, tibia, and fibula, respectively. In this study, frictional contacts with a coefficient of 0.2 were assumed at 16 potential contact regions, including the lower surface of the femoral cartilage, the upper surface of the tibial cartilage, the upper and lower surfaces of the medial and lateral meniscus, and the surfaces of four ligaments [13]. Contact simulation was performed using the generalized contact algorithm in ABAQUS [17].

Based on GROOD et al. [18], a local coordinate system for the knee joint was established, with the midpoint of the femoral condylar line as the origin. The X, Y, and Z axes defined flexion, internal/external rotation, and translational motions in six degrees of freedom. The midpoint of the femoral condyles served as the reference point, with all coupled femoral surface nodes located here, facilitating force application and data extraction for dynamic calculations. The anterior drawer test, a key clinical method for assessing knee ligament laxity and health [19], was used to validate the finite element knee joint model. This involved fixing the distal tibiofibular bone and applying a 134 N posterior thrust force to the femoral reference point to simulate the anterior drawer test. Knee joint model validation: Under a 134 N posterior thrust, the femur exhibited an anterior-posterior displacement of 4.53 mm, consistent with findings from Peña et al.[13], Gabriel et al. [20], who used cadaveric experiments and finite element models. The peak stresses in the anterior cruciate ligament, posterior cruciate ligament, medial collateral ligament, and lateral collateral ligament were 18.38, 8.20, 3.45, and 1.18 MPa, respectively. Ligament stress analysis revealed that the ACL experienced higher stress loads compared to other major ligaments, with peak stresses occurring at the tibial and femoral attachment sites. This aligns with clinical findings that the ACL primarily prevents anterior tibial displacement and that knee ligament injuries are predominantly localized at the bony attachment sites [21], [22].

ISSN: 2688-8645

1) Under the bone model, 750N longitudinal load was applied to the tip of the femur;

2) Under the muscle model, 750N longitudinal load was applied to the tip of the femur;

3) Under the bone model, a 750N longitudinal load and a 134N anterior thrust behind the tibia were applied to the tip of the femur;

4) Under the muscle model, a 750N longitudinal load and a 134N anterior thrust behind the tibia were applied to the tip of the femur.

3. Results

3.1. Stress Distribution Contrast in Knee Joint: Bone vs. Muscle Models Under 750N Loading

Under the bone model, a 750N longitudinal load applied to the tip of the femur resulted in the following stress distribution in the knee cartilage and meniscus: With an intact ACL, the peak stresses in the femoral and tibial cartilage were located in the medial anterior corner, while the peak stress in the meniscus was observed in the lateral anterior corner. When the posterior lateral bundle of the ACL was ruptured, the peak stress in the femoral cartilage shifted to the middle of the lateral side, while the peak stress in the tibial cartilage remained in the medial anterior corner. The peak stress in the meniscus was observed in the medial anterior horn. When the anterior medial bundle of the ACL was ruptured, the peak stresses in both the femoral and tibial cartilage were located in the medial anterior horn, and the peak stress in the meniscus was observed in the lateral anterior horn. In the absence of the ACL, the peak stresses in the femoral and tibial cartilage were located in the medial anterior horn, and the peak stress in the meniscus was observed in the lateral anterior horn.

Under the muscle model, the application of a 750N longitudinal load to the tip of the femur did not significantly alter the locations of peak stresses in the femoral cartilage, tibial cartilage, and meniscus compared to the bone model. By comparing the stress cloud plots of the bone and muscle models, the contribution of muscle activity to the model was quantified, as illustrated in Figures 4.

3.2. Stress Distribution Contrast in Knee Joint: Bone vs. Muscle Models Under 750N Longitudinal & 134N Anterior

Under the bone model, the application of a 750N longitudinal load combined with a 134 N anterior thrust behind the tibia to the tip of the femur did not significantly alter the locations of peak stresses in the femoral cartilage, tibial cartilage, and meniscus compared to the application of a 750N longitudinal load alone (Fig. 5). With an intact ACL, the peak stresses in the femoral and tibial cartilage were located at the medial anterior corner, while the peak stress in the meniscus was observed at the lateral anterior corner. When the posterior lateral bundle of the ACL was ruptured, the peak stress in the femoral cartilage shifted to the middle of the posterolateral side, while the peak stresses in the tibial cartilage and meniscus remained at the medial anterior corner. When the anterior medial bundle of the ACL was ruptured, the peak stresses in the femoral and tibial cartilage were located at the middle of the medial side, and the peak stress in the meniscus was observed at the middle of the lateral side. When the ACL was absent, the peak stresses in the femoral and tibial cartilage were located in the medial anterior horn, and the peak stress in the meniscus was observed in the lateral anterior horn.

Under the muscle model, the application of a 750N longitudinal load combined with a 134 N anterior thrust behind the tibia to the tip of the femur did not significantly alter the locations of peak stresses in the femoral cartilage, tibial cartilage, and meniscus compared to the bone model.

ISSN: 2688-8645

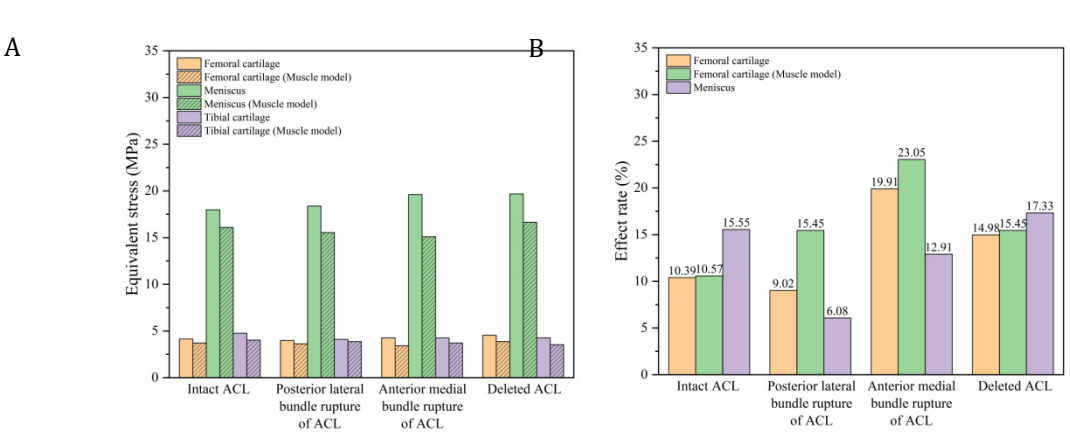

Fig 4. (A)Stress clouds of meniscus and cartilage in each group of models during 750N longitudinal loading at the tip of the femur, (B)Muscle rate of effect during 750N longitudinal loading at the tip of the femur

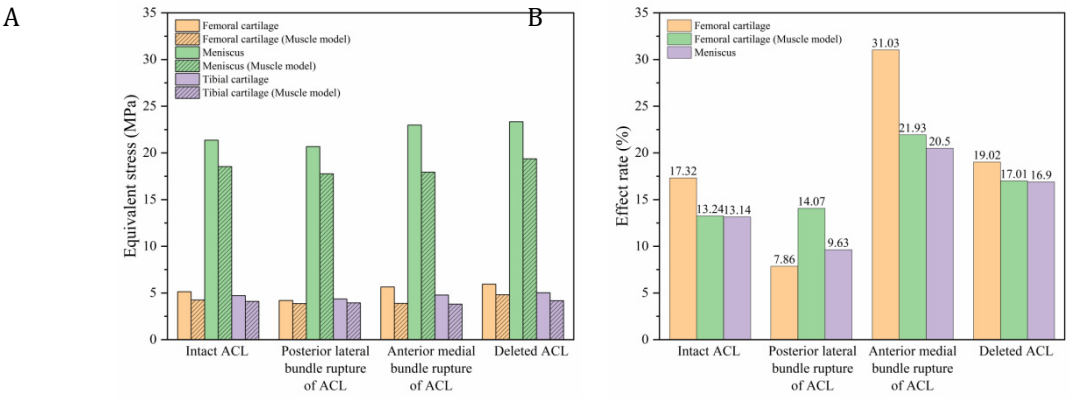

Fig 5. (A)Stress clouds of meniscus and cartilage in each group of models during 750N longitudinal load and a 134N anterior thrust behind the tibia were applied to the tip of the femur, (B)Muscle rate of effect during 750N longitudinal load and a 134N anterior thrust behind the tibia

4. Discussion

The anterior cruciate ligament plays a crucial role in maintaining knee joint stability, particularly in providing rotational and translational stability [23]. ACL injuries, often secondary to meniscal injuries, can alter the stress distribution within the knee joint, disrupting intra-articular balance and increasing the risk of knee instability and osteoarthritis [24]. Three-dimensional finite element modeling is predominantly based on noninvasive CT or MRI scans [25]. CT is more sensitive for bone imaging, while MRI is more effective for soft tissue visualization. Historically, most knee models have relied on either CT or MRI alone [25], [26]. Relying solely on CT or MRI imaging significantly reduces model accuracy, resulting in unreliable mechanical analysis of the knee joint. Therefore, this study combined CT and MRI data, utilizing CT for bone extraction and MRI for soft tissue extraction. The alignment and fusion of these imaging modalities enabled the creation of a more realistic 3D finite element model of the knee joint. In this study, CT and MRI data were integrated, with CT used for bone extraction and MRI for soft tissue extraction. The alignment and fusion of these datasets facilitated the development of a more realistic 3D finite element model of the knee joint.

This study aimed to investigate the mechanism of ACL injury and its secondary meniscal injuries by analyzing stress changes in various knee joint components following partial ACL

ISSN: 2688-8645

rupture, both with and without muscle modeling, in an extended knee state. When a 750N longitudinal load was applied to the tip of the femur, the overall meniscus stress and its peak value increased significantly in cases of anterior medial bundle rupture or complete ACL absence. However, the stress distribution of the meniscus remained relatively unchanged, consistent with the findings of YAO et al. [27]. With an intact ACL, the peak stresses in the femoral cartilage, meniscus, and tibial cartilage were 4.14, 17.98, and 4.76 MPa, respectively. In the muscle state, these values decreased to 3.71, 16.08, and 4.02 MPa, respectively, indicating a reduction in peak stresses and suggesting that muscles exert a tensile effect in the model. When the anterior medial bundle of the ACL was ruptured, the muscle's contribution to stress reduction in the femoral cartilage, meniscus, and tibial cartilage was 19.91%, 23.05%, and 12.91%, respectively, significantly higher than in the other three knee joint states. The results of this study align with previous findings [28], validating the accuracy of the three-dimensional finite element knee joint model developed in this study.

When a 750N longitudinal load combined with a 134 N anterior thrust behind the tibia was applied to the tip of the femur, the posterior tibial thrust significantly increased anterior tibial translation. Consequently, the peak stress in the lateral meniscus increased dramatically compared to the application of a 750N longitudinal load alone, resulting in elevated compressive stress on the meniscus. Under this loading condition, the most significant stress change occurred in the meniscus. The anteromedial bundle plays a critical role in limiting anterior tibial displacement during knee extension, consistent with the findings from the three-dimensional finite element knee joint model developed by XIE et al. [29]. When the anterior medial bundle of the ACL was ruptured, the muscle's contribution to stress reduction in the femoral cartilage, meniscus, and tibial cartilage was 31.03%, 21.93%, and 20.05%, respectively. This indicates that muscles undergo greater stretching during anterior medial bundle rupture. Knee over-extension exacerbates the load on the femoral cartilage and meniscus. Therefore, patients with anterior medial bundle ACL injuries should avoid prolonged standing and movements that may lead to knee over-extension, as these actions increase the risk of secondary meniscal injuries.

This study has several limitations: (1) The 3D finite element knee joint model was constructed using imaging data from a single volunteer, limiting the generalizability of the results. Further studies are required to enhance the model's applicability. (2) The model did not account for different knee flexion angles, limiting its ability to simulate various walking conditions. Future research will focus on developing a 3D finite element knee joint model incorporating multiple flexion angles to better study the mechanical behavior of the knee joint across different angles. (3) The lack of experimental data from living knee specimens makes it challenging to directly compare the results with stress changes in knee joint components during actual gait cycles. To address this, the research group is establishing a mechanical research laboratory for living knee specimens and plans to validate the findings through additional cadaveric mechanical experiments, thereby enhancing the scientific rigor and reliability of the results.

5. Conclusion

In this study, we constructed a finite element knee joint model incorporating muscles to analyze the multifaceted effects of varying degrees of ACL injuries. The results highlight the critical role of the anterior medial bundle in maintaining translational and rotational stability of the knee joint, as well as the elevated risk of meniscal injuries associated with its damage.

Therefore, in sports requiring high knee rotational stability, ACL compromise necessitates heightened vigilance for potential secondary meniscal injuries, particularly when the anterior medial bundle is ruptured, given its substantial impact on knee stability. Prompt clinical intervention and treatment are essential following such injuries to protect the meniscus and

prevent long-term complications, such as osteoarthritis. It is crucial for individuals engaged in high-risk sports to fully understand the severity of ACL injuries and implement appropriate preventive and therapeutic measures.

References

[1] Nessler T, Denney L, Sampley J. ACL Injury Prevention: What Does Research Tell Us? Curr Rev Musculoskelet Med. 2017 Sep;10(3):281-288. doi: 10.1007/s12178-017-9416-5. PMID: 28656531; PMCID: PMC5577417.

[2] Rugg C.M., Wang D., Sulzicki P., Hame S.L., Effects of prior knee surgery on subsequent injury, imaging, and surgery in NCAA collegiate athletes, Am. J. Sports Med., 2014, 42 (4), 959–964. DOI: 10.1177/0363546513519951.

[3] Ismail S.A., Button K., Simic M., Van Deursen R., Pappas E., Three-dimensional kinematic and kinetic gait deviations in individuals with chronic anterior cruciate ligament deficient knee: A systematic review and meta-analysis, Clin. Biomech. (Bristol), 2016, 35, 68–80. DOI: 10.1016/j. clinbiomech. 2016. 04.002.

[4] Akalın Y., Avcı Ö., İnce S.I., Çevik N., Şahin İ.G., Öztürk A., Comparison of cases with anterior cruciate ligament reconstruction accompanied by simultaneous medial meniscus bucket handle tear repair and isolated medial meniscus bucket handle tear repair, J. Knee Surg., 2022, 35 (11), 1242–1248. DOI: 10.1055/s-0040-1722624.

[5] Farinelli L., Meena A., Sonnery-Cottet B., Vieira T.D., Pioger C., Gigante A. et al., Increased intra-articular internal tibial rotation is associated with unstable medial meniscus ramp lesions in ACL-injured athletes: An MRI matched-pair comparative study, Arthrosc. Sports Med. Rehabil., 2023, 6 (1), 100839. DOI: 10.1016/j.asmr.2023.100839.

[6] Kalifis G., Raoulis V., Panteliadou F., Liantsis A., D'Ambrosi R., Hantes M., Long-term follow-up of bucket-handle meniscal repairs: chondroprotective effect outweighs high failure risk, Knee Surg. Sports Traumatol. Arthrosc., 2022, 30 (7), 2209–2214. DOI: 10.1007/s00167-021-06787-2.

[7] Qi Y., Sun H., Fan Y., Li F., Wang Y., Ge C., Three-dimensional finite element analysis of the influence of posterior tibial slope on the anterior cruciate ligament and knee joint forward stability, J. Back Musculoskelet. Rehabil., 2018, 31 (4), 629-636. DOI: 10.3233/BMR-169703.

[8] Ramaniraka N.A., Terrier A., Theumann N., Siegrist O., Effects of the posterior cruciate ligament reconstruction on the biomechanics of the knee joint: a finite element analysis, Clin. Biomech. (Bristol), 2005, 20 (4), 434-442. DOI: 10.1016/j.clinbiomech.2004.11.014.

[9] Nikkhoo M., Hassani K., Tavakoli Golpaygani A., Karimi A., Biomechanical role of posterior cruciate ligament in total knee arthroplasty: A finite element analysis, Comput. Methods Programs Biomed., 2020, 183, 105109. DOI: 10.1016/j.cmpb.2019.105109.

[10] Park H.J., Kim S.S., Lee S.Y., Park N.H., Ahn J.H., Chung E.C. et al., Comparison between arthroscopic findings and 1.5-T and 3-T MRI of oblique coronal and sagittal planes of the knee for evaluation of selective bundle injury of the anterior cruciate ligament, AJR Am. J. Roentgenol., 2014, 203 (2), W199-W206. DOI: 10.2214/AJR.13.11571.

[11] Grevnerts H.T., Sonesson S., Gauffin H., Ardern C.L., Stålman A., Kvist J., Decision Making for Treatment After ACL Injury From an Orthopaedic Surgeon and Patient Perspective: Results From the NACOX Study, Orthop. J. Sports Med., 2021, 9 (4), 23259671211005090. DOI: 10.1177/ 232596 71211005090.

[12] Konrads C., Döbele S., Ateschrang A., Ahmad S.S., Outcome of anterior cruciate ligament reconstruction in children and adolescents: A retrospective study, J. Clin. Orthop. Trauma, 2020, 13, 46-49. DOI: 10.1016/j.jcot.2020.08.022.

[13] Peña E., Calvo B., Martínez M.A., Doblaré M., A three-dimensional finite element analysis of the combined behavior of ligaments and menisci in the healthy human knee joint, J. Biomech., 2006, 39 (9), 1686-1701. DOI: 10.1016/j.jbiomech.2005.04.030.

[14] Li Yang, Sang Jianbing, Ao Rihan, et al. Research on the Inversion Method of Hyperelastic Constitutive Parameters of Skeletal Muscle Based on Simulation and Intelligent Algorithm [J] Acta Mechanica Sinica, 2021,53(05):1449-1456.

[15] Zhang X., Jiang G., Wu C., Woo S.L., A subject-specific finite element model of the anterior cruciate ligament, Annu. Int. Conf. IEEE Eng. Med. Biol. Soc., 2008, 2008, 891-894. DOI: 10.1109/ IEMBS. 2008. 4649297.

[16] Homyk A., Orsi A., Wibby S., Yang N., Nayeb-Hashemi H., Canavan P.K., Failure locus of the anterior cruciate ligament: 3D finite element analysis, Comput. Methods Biomech. Biomed. Engin., 2012, 15 (8), 865-874. DOI: 10.1080/10255842.2011.565412.

[17] ABAQUS, Version 6.10 Documentation, ABAQUS Analysis Manual, Simulia, Dassault Systèmes, 2010.

[18] Grood E.S., Suntay W.J., A joint coordinate system for the clinical description of three-dimensional motions: application to the knee, J. Biomech. Eng., 1983, 105 (2), 136-144. DOI: 10.1115/1.3138397.

[19] Skinner H., Current Diagnosis and Treatment in Orthopedics, McGraw-Hill Professional Publishing, 2006.

[20] Gabriel M.T., Wong E.K., Woo S.L., Yagi M., Debski R.E., Distribution of in situ forces in the anterior cruciate ligament in response to rotatory loads, J. Orthop. Res., 2004, 22 (1), 85-89. DOI: 10. 1016/ S0736-0266(03)00133-5.

[21] Song Y., Debski R.E., Musahl V., Thomas M., Woo S.L., A three-dimensional finite element model of the human anterior cruciate ligament: a computational analysis with experimental validation, J. Biomech., 2004, 37 (3), 383-390. DOI: 10.1016/S0021-9290(03)00261-6.

[22] Sherman M.F., Lieber L., Bonamo J.R., Podesta L., Reiter I., The long-term followup of primary anterior cruciate ligament repair. Defining a rationale for augmentation, Am. J. Sports Med., 1991, 19 (3), 243-255. DOI: 10.1177/036354659101900307.

[23] Uğur L., Comparison of reaction forces on the anterior cruciate and anterolateral ligaments during internal rotation and anterior drawer forces at different flexion angles of the knee joint, Int. J. Med. Robot., 2017, 13 (4), e1815. DOI: 10.1002/rcs.1815.

[24] Dejour D., Pungitore M., Valluy J., Nover L., Saffarini M., Demey G., Preoperative laxity in ACL-deficient knees increases with posterior tibial slope and medial meniscal tears, Knee Surg. Sports Traumatol. Arthrosc., 2019, 27 (2), 564-572. DOI: 10.1007/s00167-018-5180-3.

[25] Gardiner J.C., Weiss J.A., Subject-specific finite element analysis of the human medial collateral ligament during valgus knee loading, J. Orthop. Res., 2003, 21 (6), 1098-1106. DOI: 10.1016/S0736-0266(03)00113-X.

[26] Jogi S.P., Thaha R., Rajan S., Mahajan V., Venugopal V.K., Singh A. et al., Model for in-vivo estimation of stiffness of tibiofemoral joint using MR imaging and FEM analysis, J. Transl. Med., 2021, 19 (1), 310. DOI: 10.1186/s12967-021-02977-1.

[27] Yao J., Snibbe J., Maloney M., Lerner A.L., Stresses and strains in the medial meniscus of an ACL deficient knee under anterior loading: a finite element analysis with image-based experimental validation, J. Biomech. Eng., 2006, 128 (1), 135-141. DOI: 10.1115/1.2132373.

[28] Zhang K., Li L., Yang L., Shi J., Zhu L., Liang H. et al., Effect of degenerative and radial tears of the meniscus and resultant meniscectomy on the knee joint: a finite element analysis, J. Orthop. Translat., 2019, 18, 20-31. DOI: 10.1016/j.jot.2018.12.004.

[29] Xie F., Yang L., Guo L., Wang Z.J., Dai G., A study on construction three-dimensional nonlinear finite element model and stress distribution analysis of anterior cruciate ligament, J. Biomech. Eng., 2009, 131 (12), 121007. DOI: 10.1115/1.4000167.